Far-infrared optical properties of superconducting $Bi_2Sr_2CaCu_2O_x$ films

A. M. Rao,* P. C. Eklund, and G. W. Lehman
Department of Physics and Astronomy, University of Kentucky, Lexington, Kentucky 40506

D. W. Face†
Center for Materials Science and Engineering, Massachusetts Institute of Technology, Cambridge, Massachusetts 02139

G. L. Doll‡
Department of Physics, Massachusetts Institute of Technology, Cambridge, Massachusetts 02139

G. Dresselhaus
Francis Bitter National Magnet Laboratory, Massachusetts Institute of Technology, Cambridge, Massachusetts 02139

M. S. Dresselhaus
Department of Electrical Engineering and Computer Science and Department of Physics, Massachusetts Institute of Technology, Cambridge, Massachusetts 02139
(Received 18 December 1989)

The optical reflectance of thin superconducting $Bi_2Sr_2CaCu_2O_x$ (Bi 2:2:1:2) films has been studied in the frequency range 80–48 000 cm^{-1} and the temperature range 5 K $< T <$ 300 K. Since the film thickness d is less than the optical skin depth δ, the reflectance from the film-substrate ($SrTiO_3$) interface must be considered in the interpretation of the experimental results. The dielectric function of the superconductor is calculated with use of the model of Leplae, which takes into account the effect of the quasiparticle lifetime. Structure in the reflectivity spectra is identified with Bi 2:2:1:2 phonons, $SrTiO_3$ substrate phonons, and for $T < T_c$, evidence for a superconducting gap is observed. The gap at $T = 5$ K was found to be $2\Delta = 35 \pm 5$ meV $\simeq 6k_B T_c$, in good agreement with previous tunneling studies.

I. INTRODUCTION

It is expected that the most important electronics applications of high-T_c materials will come from thin-film devices and interconnects. Thus, it is important to be able to characterize the properties of thin-film high-T_c materials and, in particular, to determine a value for the superconducting gap 2Δ. Optical and tunneling experiments[1–6] can both, in principle, determine values for 2Δ, but each has much different probe depths. Superconducting gap values in the high-T_c materials obtained from tunneling measurements range from 20 to 120 meV,[1–4] while the optical experiments yield 2Δ values in the range 8–60 meV.[5,6] Some controversy exists however, as to whether structure in the data has been properly identified with 2Δ.[7] From tunneling experiments on single-crystal $Bi_2Sr_2CaCu_2O_x$, Miyakawa *et al.*[1–3] estimated 2Δ to be 44 meV, and a value of 50 meV was reported by Lee *et al.*[4] also on the basis of tunneling data.

The far-infrared probe depth (or skin depth) in high-T_c materials is sufficiently deep that it can easily exceed the film thickness. When this is the case, the boundary (or interface) between the film and substrate must be included in the data analysis, if quantitative results are to be obtained from the spectra. For the $Bi_2Sr_2CaCu_2O_x$ (Bi 2:2:1:2) films studied here, we estimate that a film thickness $d > 1$ μm is necessary to justify neglect of the substrate dielectric function in the data analysis. This 1 μm thickness might be a factor of 5–10 larger than the desirable film thickness, depending on the application. To our knowledge, this is the first study to estimate 2Δ from the near-normal incidence reflectance measurements of high-T_c superconducting thin films deposited on a planar substrate. Recently, Hughes *et al.*[8] reported far-infrared transmission measurements of Bi (2:2:1:2) films on MgO substrates.

In this paper we present the results of optical reflectance studies on thin ($d \leq 0.25$ μm) films of $Bi_2Sr_2CaCu_2O_x$ extending from the far-infrared to the ultraviolet (80 $cm^{-1} < \omega <$ 48 000 cm^{-1}) and in the temperature range 5 K $< T <$ 300 K. The dielectric function of the film in the superconducting state is calculated according to the model of Leplae[9] which extends the calculation of Mattis and Bardeen[10] to include effects of the quasiparticle lifetime τ on the optical response.

II. EXPERIMENT

A. Samples

Thin films of $Bi_2Sr_2CaCu_2O_8$ on [100] $SrTiO_3$ substrates were prepared at the MIT Center for Materials Science and Engineering, by reactive, magnetically enhanced, triode sputtering using three separate metal

sources (Sr, Ca, and Cu-Bi). The sputtering system consisted of an 18 inch diameter stainless steel chamber with three triode sputter guns installed in a triangular arrangement with each gun pointed at the substrate holder. The distance between the sputtering guns and the substrate was 25 cm, and oxygen gas (99.995% pure) was introduced near the growing films via a gas inlet near the substrate holder. A rotating substrate was installed to achieve a uniform composition to within 1% over a 3.5 inch diameter area. Due to the reactivity of Ca and Sr with air, these sources were stored and handled in an inert environment prior to placing them in the vacuum system. All three sources were presputtered for at least 45 min before the film deposition, in order to achieve their equilibrium sputtering rates. After the deposition, the substrates were quickly transferred to an alumina boat and inserted into a standard quartz tube furnace for annealing. A thickness monitor placed close to the substrate holder during deposition indicated that the film thickness was ~ 0.25 μm. The films were annealed in the furnace with 20% O_2/Ar mixture at a flow rate of 1.4 l/min. The temperature was increased linearly (28 °C/min) up to about 870 °C and held at that temperature for about 30 min. The films were then quickly cooled in oxygen back to room temperature and removed from the furnace tube.

The resistivity of the two thin-film samples (referred herein as *A* and *B*) was measured by the standard four-probe method using silver paint contacts. Room-temperature resistivity measurements yielded ~ 1480 $\mu\Omega$ cm for sample *A* and 2672 $\mu\Omega$ cm for sample *B*. The ratio of the resistivities at 295 and 110 K was ~ 2 for sample *A* and ~ 1.65 for sample *B*. The midpoint of the superconducting transition was found to be 67 K and 73 K, with a "zero" resistance temperature of ~ 61 K and ~ 66 K for sample *A* and sample *B*, respectively. X-ray diffraction scans revealed that the films were predominantly single phase, and oriented such that the crystallographic tetragonal *c* axis was normal to the substrate. Scanning electron microscopy (SEM) micrographs of the films showed platelike grains, characteristic of the superconducting phase. Rutherford backscattering spectroscopy (RBS) measurements on the samples showed the composition of $Bi_{2.0}Sr_{2.0}Ca_{1.0}Cu_{2.1}O_x$ for sample *A* and $Bi_{2.0}Sr_{2.2}Ca_{1.0}Cu_{2.5}O_x$ for sample *B*. The samples were most likely oxygen deficient, i.e., $x < 8$, though the exact oxygen stoichiometry was not determined.

B. Spectrometers

The reflectance was measured using two spectrometers: (i) the Perkin-Elmer model 88 prism-based instrument [2400 cm^{-1} (0.3 eV) $< \omega <$ 48 000 cm^{-1} (6 eV)] and (ii) the modified Digilab FTS 80 Fourier-transform spectrometer equipped with a triglycine sulfate (TGS) detector (400–4000 cm^{-1}) and a Si bolometer detector (IR Labs, Arizona) (20–600 cm^{-1}). The normal incidence reflectance was measured relative to an adjacent standard mirror whose front surface was accurately coplanar with that of the film. A MgF_2 coated Al mirror and Au mirror were used in the intervals 2400 cm^{-1} $< \omega <$ 48 000 cm^{-1} and 50 cm^{-1} $< \omega <$ 4000 cm^{-1}, respectively. Data were taken for $\omega < 4000$ cm^{-1} in an exchange-gas He cryostat (MD4 Oxford Instruments) operating in the temperature range $5 < T < 300$ K equipped with ZnSe and polyethylene cold windows. The sample and standard were thermally attached to a cold finger suspended from above by a stainless steel rod in a ^{4}He exchange gas. The Au mirror, or the sample, were centered in the optical beam by translating the rod parallel to the vertical cryostat axis, out of the top of the cryostat through a sliding O-ring seal. Sample temperatures were monitored by a Si diode thermometer, heat sunk to the cold finger.

C. Data analysis including substrate

The geometry of the thin film on an infinite substrate is shown in Fig. 1. Since the film is optically thin, multiple internal reflections and absorption within the film have to be considered in the analysis. An electromagnetic wave, with its field polarized along the *y* direction, is normally incident on the planar structure and propagates along the *z* direction, $E_y(z)$. In the three regions defined in Fig. 1, we can write

$$E_y(z) = e^{ik_0 z} - re^{-ik_0 z} \quad \text{for } z \le 0 ,$$

$$E_y(z) = A_f e^{ik_f z} + B_f e^{ik_f (d-z)} \quad \text{for } 0 \le z \le d , \tag{1}$$

$$E_y(z) = te^{ik_s (z-d)} \quad \text{for } z \ge d ,$$

where the incident wave propagates along *z* with unit intensity (i.e., the sample plane is the *xy* plane). The wave vector is written as $k = \omega n / c$, where *n* is the complex refractive index and the subscripts 0, *f*, and *s* refer to the vacuum, film, and substrate, respectively. Expressions for *r* and *t* can be obtained by applying the usual boundary conditions that $E_y(z)$ and dE_y/dz are continuous at the boundary $z = 0$ (vacuum film) and $z = d$ (film sub-

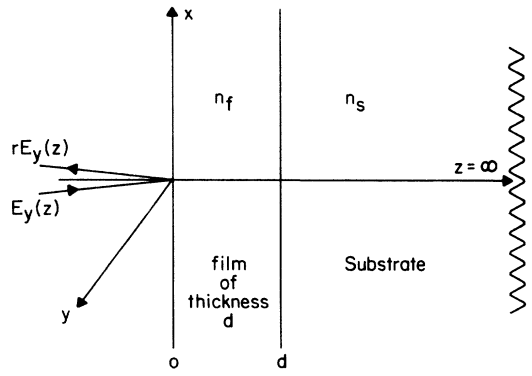

FIG. 1. Geometry of the $Bi_2Sr_2CaCu_2O_x$ thin film on a $SrTiO_3$ substrate. The incident electromagnetic wave is polarized along the *y* direction and propagates in the *z* direction. The film thickness is *d* and its optical response is characterized by n_f. The substrate is infinitely thick and its optical response is characterized by n_s.

strate). The result for the reflectance amplitude r is

$$r=\frac{(n_f-1)-\Gamma(n_f+1)}{(n_f+1)-\Gamma(n_f-1)}\ , \tag{2}$$

where

$$\Gamma=\frac{(n_f-n_s)}{(n_f+n_s)}e^{(2in_f\omega d/c)}\ . \tag{3}$$

Thus it is seen that when the film is optically thick [$\mathrm{Im}(n_f)d \gg 1$], then $\Gamma \rightarrow 0$ and the thick-film result is obtained.

For most high-T_c films $d < 1$ μm, and therefore Eq. (2) must be used to calculate the reflectivity $R=|r|^2$ and to compare with the experimental data. The values of R and of Γ will therefore depend on both the film and substrate dielectric function $\epsilon_f=n_f^2$ and $\epsilon_s=n_s^2$. High-T_c materials are usually prepared on insulating substrates such as $SrTiO_3$, MgO, or Y-stabilized ZrO_2. One-phonon infrared absorption dominates the dielectric function of these substrate materials in the infrared, and this contribution is given by[11]

$$\epsilon_s(\omega)=\epsilon_\infty+\sum_{j=1}^{p}\frac{S_j}{\omega_j^2-\omega^2-i\Gamma_j\omega}\ , \tag{4}$$

where there are p ($q=0$) ir-active modes, ϵ_∞ represents the electronic contribution to the ir absorption, and S_j, ω_j, and Γ_j are, respectively, the oscillator strength, frequency, and the damping for the jth mode.

Equation (4) is the form usually used for describing the contribution from the independent or the uncoupled phonons. However, in the case of $SrTiO_3$, Barker and Hopfield have shown that a better fit to the experimental data is obtained if the lowest and the highest frequency modes or phonons are coupled.[12] To complicate matters somewhat further, the lowest frequency phonon in $SrTiO_3$ exhibits a strong softening with decreasing temperature, consistent with a low-temperature ferroelectric state.[13,14] Our dielectric function $\epsilon_s(\omega)$ for $SrTiO_3$ is thus calculated according to the coupled mode equations in Ref. 12 for the parameters given in Table I of Ref. 12.

III. RESULTS

A. Normal state

We first describe the data analysis for the film in the normal state. The dielectric function of the film in the normal state is described in the usual way by

$$\epsilon_N=\epsilon_\infty+\epsilon_{\mathrm{phonon}}+\epsilon_{\mathrm{Drude}}\ , \tag{5}$$

where $\epsilon_{\mathrm{phonon}}$ assumes the same functional form as in Eq. (4), and the term $\epsilon_{\mathrm{Drude}}$ is the free carrier contribution in the Drude approximation given by

$$\epsilon_{\mathrm{Drude}}=\frac{-\omega_p^2}{\omega(\omega+i/\tau)}\ , \tag{6}$$

where ω_p is the plasma frequency and τ is the free carrier scattering time (assumed to be a real constant).

In Fig. 2 we show the reflectance spectra for sample A in the frequency range $0<\omega<1500$ cm^{-1} for temperatures in the range 5 K $<T<$ 300 K. The midpoint of the resistive transition for sample A is $T_c=67$ K. The most prominent structure in the spectra is at $\sim$540 cm^{-1} and is due to a $SrTiO_3$ ir phonon at $\omega=544$ cm^{-1}.[12] The reflectance spectra for sample A were measured with an instrument resolution of $\sim$4 cm^{-1}, and therefore the structure at $\sim$170 cm^{-1} of the $SrTiO_3$ phonon was not resolved in the reflectance of sample A. However, the $\sim$170 cm^{-1} feature in $SrTiO_3$ was resolved in subsequent experiments with higher instrument resolution in sample B and is shown as an inset in Fig. 2. Since no difference was observed in the reflection spectra of samples A and B for frequencies above point P, we measured the reflection of sample B for various temperatures, but only in the frequency range below the point P. The arrows in Fig. 2 (inset) indicate the soft mode feature for $SrTiO_3$. For the reflectance at 300 K, both the data and a least square smoothing of the data are shown. The noise in the spectrum for $T=300$ K is also typical of the low-temperature reflectance spectra, and so for clarity, we show only the smoothed data for $T<72$ K data.

The normal-state spectra for ($T>72$ K) exhibit a

TABLE I. Fitting parameters for 5–90 K and 300 K reflectance data obtained from sample A. Two phonons were introduced to fit the data. The temperature-dependent reflectance of sample A for $T<72$ K (Fig. 2) was fit with a temperature-dependent superconducting gap parameter while the phonons remain essentially constant for the $T=90$ K spectrum through the $T=5$ K spectrum.

Phonon	Parameter	This work $T=5$–90 K	This work $T=300$ K	Reedyk *et al.* (Ref. 15) $T=100$ K
	ϵ_∞	5.2	5.2	
	ρ_0 ($\mu\Omega$ cm)	1969	2953	
	ρ_{dc} ($\mu\Omega$ cm)	740@100 K	1480	33
1	ω_p (cm^{-1})	3630	2178	2800
	ω_n (cm^{-1})	242	242	412
	γ_n (cm^{-1})	226	202	153
2	ω_p (cm^{-1})	4033	6453	13800
	ω_n (cm^{-1})	726	726	996
	γ_n (cm^{-1})	1613	1613	1180

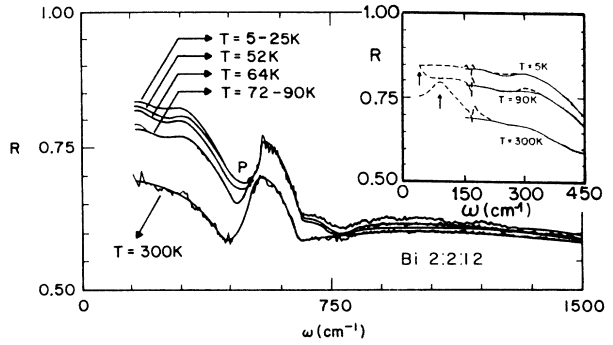

FIG. 2. Temperature-dependent reflectivity spectra of sample A. For the $T=300$ K spectrum, both the raw data and the smoothed data are shown. For $T\leq 90$ K, only the smoothed data are shown. In the region below the pinning point P the spectra fan out at low temperatures. The spectra superimpose between 72 $K\leq T\leq 90$ K and between 5 K $\leq T\leq 25$ K. In the inset, the smoothed data of sample B (dashed line) are compared with those of sample A (solid line). The structure at ~ 170 cm^{-1} in the smoothed data of sample B is due to the $SrTiO_3$ substrate which was not resolved in the spectrum of sample A due to lower instrument resolution. The arrows in the inset indicate the soft mode feature for $SrTiO_3$.

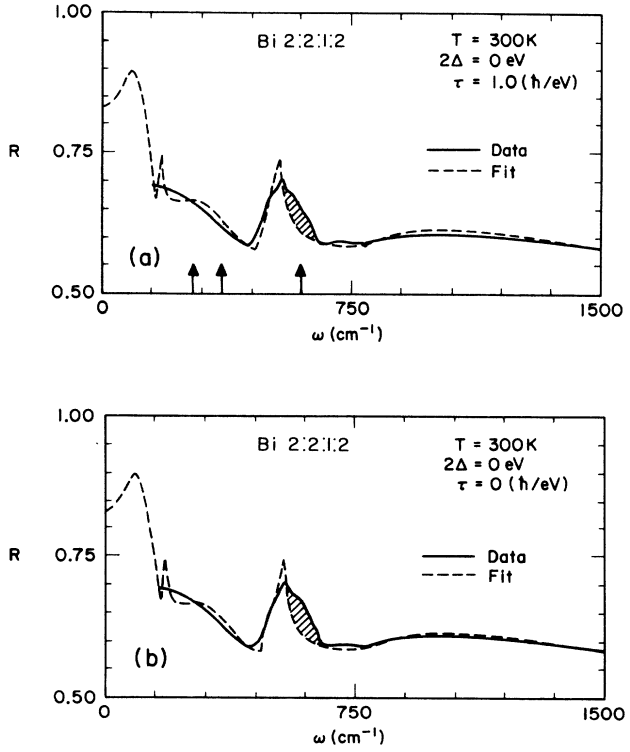

FIG. 3. Fits to the $T=300$ K data calculated according to Eqs. (2)–(6) are shown. The parameters for the Bi (2:2:1:2) film are listed in Table I. In (a) $\tau=1\hbar$/eV while in (b) $\tau\sim 0\hbar$/eV. The arrows indicate the positions of the in-plane phonons according to Piro *et al.* (Ref. 16) Structures at $\omega=90$, 170, and 540 cm^{-1} are due to the $SrTiO_3$ substrate (see text).

significant increase in the overall reflectance when the sample is cooled from 300 K to 90 K. This rise in R below 1000 cm^{-1} is due both to an increase in the free carrier scattering time τ, consistent with the temperature dependence of the resistivity ρ, as well as to changes in the substrate dielectric function.[14] Between 90 and 72 K the spectra nearly superimpose. The normal-state reflectance for sample B was identical to that of sample A, except for better resolution of the $SrTiO_3$ phonon mode near 170 cm^{-1}.

In Figs. 3 and 4 we show the fits to the $T=300$ K and 90 K data, respectively, calculated according to Eqs. (2)–(6). The fitting parameters for the Bi (2:2:1:2) film are listed in Table I. Values for the zero frequency optical conductivity $\sigma_0=\omega_p^2\tau/4\pi$ and the dc conductivity σ_{dc} obtained from transport measurements are listed in Table I and are in reasonable agreement with each other. The ratios of the conductivities at 100 and 300 K compare favorably: $\sigma_0(100/300)=1.5$ and $\sigma_{dc}(100/300)=2$. Two Bi (2:2:1:2) phonons at $\omega_1=242$ cm^{-1} and $\omega_2=726$ cm^{-1} were introduced to fit the data. These phonon frequencies are lower than the values of $\omega_1=412$ cm^{-1} and $\omega_2=996$ cm^{-1} reported recently by Reedyk *et al.*[15] for Bi (2:2:1:2) single-crystal samples and Hughes *et al.*[8] for the Bi (2:2:1:2) films on MgO substrates. By correlating the phonon modes associated with a homologous set of equivalent atoms in 1:2:3 and 2:2:1:2 compounds, Piro *et al.*[16] made tentative phonon assignments in their infrared reflectance measurements on polycrystalline Bi (2:2:1:2). They reported three ir-active in-plane phonons at 275, 360, and 600 cm^{-1}, one more than that reported by Reedyk *et al.*[15] and Hughes *et al.*[8] A fit incorporating three oscillators to our data did not improve the fit appreciably. We believe that the misfit represented by the shaded region in Fig. 3 is primarily due to an imperfect description of the substrate refractive index $n_s(\omega)$.

As shown in Figs. 3 and 4, the normal-state spectra at both 300 and 90 K could be fit well with either $\tau=0$ or $\tau=1$ ($\hbar$/eV). This implies that the normal-state spectra can be fit well with a frequency-dependent τ (for $0<\tau\leq 1\hbar$/eV), unlike the results of Collins *et al.*[17] To obtain convergence in the actual fits, we have taken $\tau=10^{-5}$ ($\hbar$/eV) to represent $\tau=0$. A scattering rate $1/\tau$ of 650 cm^{-1} (or $\tau\sim 12\hbar$/eV) at 100 cm^{-1} and a $1/\tau\sim 300$ cm^{-1} (or $\tau\sim 2.7\hbar$/eV) at 2500 cm^{-1} was used in their analysis of the normal-state conductivity of $YBa_2Cu_3O_7$. Reedyk *et al.*[15] observed that if their normal-state optical conductivity was analyzed with a frequency-dependent scattering rate, then $1/\tau$ was found to increase from 200 cm^{-1} (or $\tau\sim 40\hbar$/eV) at low frequency to 1500 cm^{-1} (or $\tau\sim 5\hbar$/eV) at 700 cm^{-1}.

The separation of the substrate and film structure in the reflectance is best shown in Fig. 5, where we plot the calculated reflectance of a Bi (2:2:1:2) film on $SrTiO_3$ at 5 K with the film thickness as a parameter. The structure at $\omega=90$, 170, and 540 cm^{-1} due to the $SrTiO_3$ phonons gradually disappears as the film thickness increases from $d=0.25$ μm to $d=1.0$ μm. The calculated differences in R for $d>1$ μm are too small to be seen in Fig. 5.

B. Superconducting state

The optical response of the film for $T<T_c$ was calculated in the effective medium approximation (EMA) to

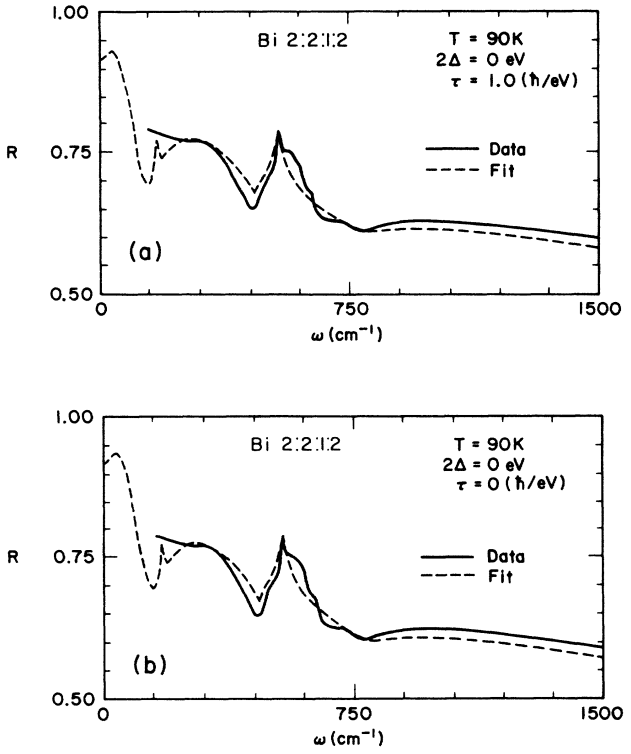

FIG. 4. Fits to the $T=90$ K data calculated according to Eqs. (2)–(6) are shown. The parameters for the Bi (2:2:1:2) film are listed in Table I. In (a) $\tau=1\hbar/\text{eV}$ while in (b) $\tau\sim 0\hbar/\text{eV}$.

account for the effect of some fraction η of the film which might remain normal (or not exhibit a superconducting gap).[18] The film conductivity σ_f is given in the EMA by

$$\eta\frac{\sigma_f-\sigma_N}{\sigma_f+2\sigma_N}+(1-\eta)\frac{\sigma_f-\sigma_S}{\sigma_f+2\sigma_S}=0\ , \tag{7}$$

where σ_N and σ_S refer to the optical conductivity of the normal and superconducting components, respectively. The fitting parameters used above for σ_N were identical to the $T=90$ K parameters in Table I, whereas for σ_S we used the description formulated by Leplae[9] and parametrized by a gap $2\Delta=\hbar\omega_g$, conductivity σ_0, and quasiparticle lifetime τ. In the limit $\tau\to 0$, which is referred to as the "dirty limit," Leplae's result was found to reduce to the earlier result of Mattis and Bardeen.[10] This is shown in the Appendix along with the transformations of Leplae's results into expressions more suitable for numerical analysis. In Figs. 6(a) and 6(b) we show the effect of varying the gap 2Δ and the normal-state fraction η, respectively, on the calculated reflectance R. The curves are calculated with the best fit $T=5$ K parameters listed in Table I. For the low-temperature reflectivity data (90 to 5 K) the refractive index n_s of $SrTiO_3$ is obtained from the 300 K parameters as listed in Table I of Ref. 5 with one change: The lowest frequency mode was softened from 88 to 40 cm^{-1} consistent with the data of Barker and Tinkham.[14] In the analysis of the reflectance spectra for $T<90$ K, we assumed that the lowest frequency mode in $SrTiO_3$ does not soften further, as the temperature of the sample is lowered. As shown in Fig. 6(a), the curves are pinned at ~ 450 cm^{-1}, near the highest frequency $SrTiO_3$ phonon mode and rise with a slope which is sensitive to the value of 2Δ. The effect of η in Fig. 6(b) is to lower the overall magnitude of R as a larger normal-state fraction is added to the composite conductivity. It is clear from Figs. 6(a) and 6(b) that a large value for η reduces the sharp enhancement in the reflectance of the superconducting sample, thus making it

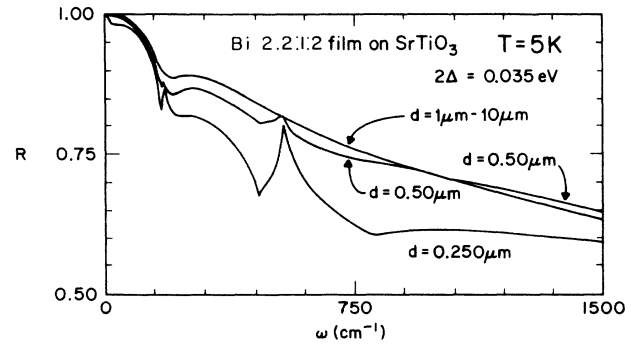

FIG. 5. Plots of calculated reflectance of a Bi (2:2:1:2) film on $SrTiO_3$ at 5 K for different film thicknesses d. The structure at $\omega=90$, 170, and 540 cm^{-1} due to the $SrTiO_3$ phonons gradually disappears as the film thickness increases from $d=0.25$ to $d=1.0$ μm.

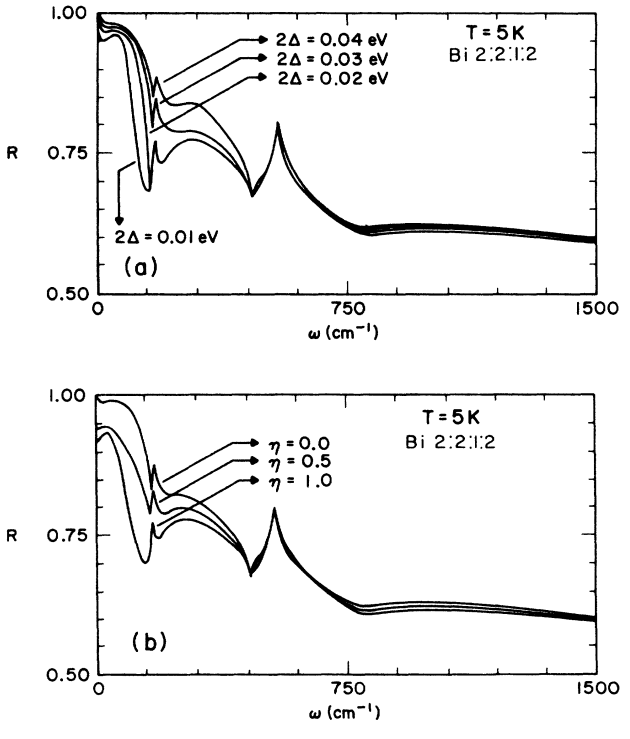

FIG. 6. (a) Plots of calculated reflectance for different gap energies 2Δ with the 5 K fitting parameters listed in Table I and $\tau=1\hbar/\text{eV}$. (b) Plots of calculated reflectance for different normal-state fractions η obtained with $\tau=1\hbar/\text{eV}$ and the 5 K fitting parameters listed in Table I.

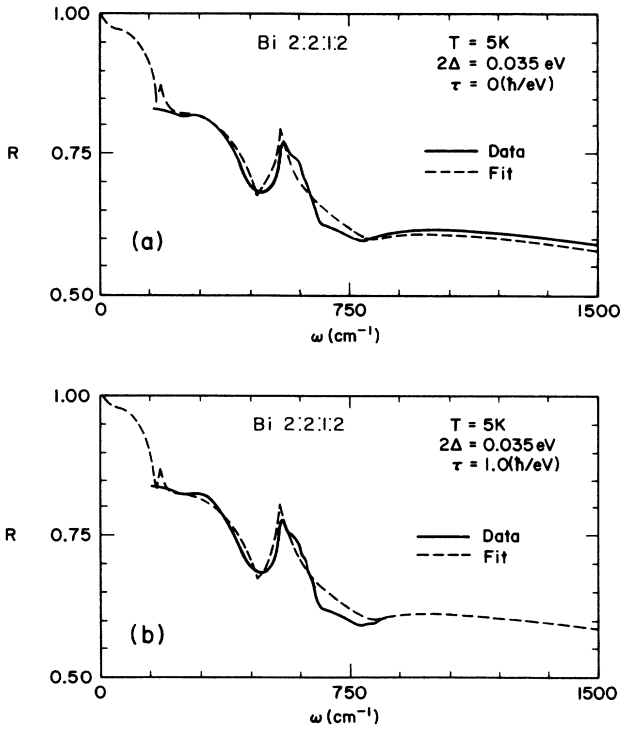

FIG. 7. The smoothed reflectance data for sample A at $T=5$ K and the dashed curve obtained from the fitting parameters listed in Table I and $2\Delta=35$ meV, with $\tau\sim 0\hbar$/eV in (a), while $\tau=1\hbar$/eV in (b).

hard to quantitatively determine the superconducting gap. Also, the short coherence length of the superconducting phase may be partly responsible for the smearing of the superconducting gap. The sudden increase in the reflectance of our Bi (2:2:1:2) film for frequencies below point P (see Fig. 2), which is the superconducting gap region, suggests that η for our film is small (~ 0.1). This probably indicates that some of the grains in our Bi (2:2:1:2) film have a stoichiometry which is not sufficiently close to that needed to superconduct.

In Fig. 7 we display the fit to the $T=5$ K spectrum of sample A. The solid and dashed lines represent the experimental and calculated results, respectively, and a

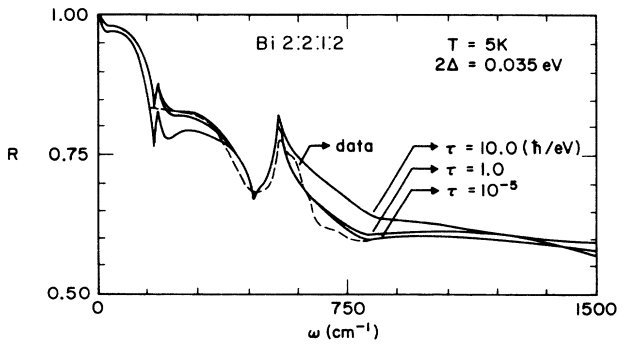

FIG. 8. Plots of calculated reflectance for different values of τ using the $T=5$ K fitting parameters listed in Table I. The dashed curve represents the $T=5$ K data. The $\tau=0$ and $\tau=1\hbar$/eV results are in the dirty limit [i.e., $\omega_g\tau\ll 1$].

comparison of these curves shows the degree of agreement achieved. The Bi (2:2:1:2) phonon parameters are the same as found for the $T=72$ K (normal-state) spectra. The 5 K data along with the calculated curves corresponding to $\tau=0$, 1, and $10\hbar$/eV are indicated in Fig. 8. The calculated curves share the same value for the gap $2\Delta=35$ meV and the normal-state fraction $\eta=0.1$. The fit obtained with $\tau=10\hbar$/eV is broader than that obtained for $\tau=1\hbar$/eV in the region around the $SrTiO_3$ phonon at 540 cm^{-1}. At higher ω, the fit obtained with $\tau=10\hbar$/eV yields lower reflectance values than those obtained with $\tau=1\hbar$/eV. We also find that the superconducting-state spectra can be fit equally well with $\tau=0$ and $\tau=1\hbar$/eV, but a poor fit is obtained for $\tau=10\hbar$/eV. The corresponding range of values for $\omega_g\tau$ obtained from our fits to the 5 K data is $0\le\omega_g\tau\le 0.035$. These data suggest that the sample is well described in the dirty-limit ($\omega_g\tau\ll 1$) rather than in the clean-limit ($\omega_g\tau\gg 1$) approximation. For comparison $\omega_g\tau=0.09$ in NbN films as reported by Karecki *et al.*[19,20] and $\omega_g\tau=0.2$ in Pb (see the Appendix in Ref. 19).

The reflectivity in a BCS metal shows a prominent edge in the superconducting gap region for $\omega<\omega_g$ above which the reflectance becomes unity, and then gradually falls to join the normal-state (metal) value for frequencies above the superconducting gap. In the ceramic samples of high-T_c superconductors, Bonn *et al.*[21] and Sherwin *et al.*[22] showed that the zero crossing in ϵ_1 can give rise to this characteristic edge. They, however, observed that a positive contribution to ϵ_1 in $La_{2-x}Sr_xCuO_4$ could arise either from the presence of a strong midinfrared band, or a strong phonon absorption near 250 cm^{-1}. Although there is phonon absorption in the superconducting gap region, the temperature-dependent reflectance spectra shown in Fig. 2 can be fit rather well with a temperature-

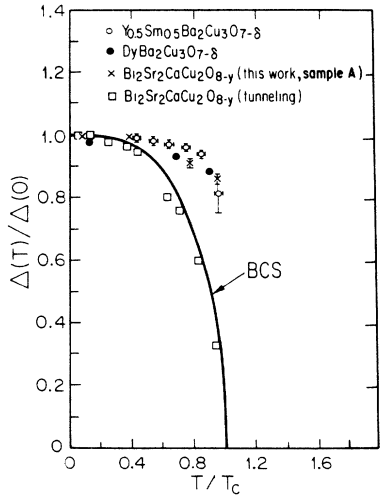

FIG. 9. Temperature dependence of the reduced gap for sample A as a function of the reduced temperature. Sample B did not exhibit any temperature dependence of 2Δ for $T<T_c$. The solid curve represents the results from the BCS theory. Data obtained from other high-T_c ceramic samples and from tunneling measurements on a Bi (2:2:1:2) sample are also plotted (see text).

dependent gap parameter, while the phonon contributions remain essentially constant as T is lowered from 90 to 5 K.

In Fig. 9 we plot our results for the reduced gap obtained from analysis of spectra for sample A below 70 K versus the reduced temperature. Also shown in the plot are data for the temperature dependence of the gap for ceramic $Y_{0.5}Sm_{0.5}Ba_2Cu_3O_{7-\delta}$ and $DyBa_2Cu_3O_{7-\delta}$ samples, obtained from infrared spectroscopy by Wittlin *et al.*,[23] and for the single-crystal $Bi_2Sr_2CaCu_2O_{8-x}$ from tunneling experiments by Lee *et al.*[4] The solid curve in Fig. 9 represents the reduced gap predicted by the BCS theory. Our data on sample A are consistent with the temperature dependence of the gap obtained from the optical data of Wittlin *et al.*[23] Sample B did not exhibit any temperature dependence of the gap for $T < T_c$, although the value of the superconducting gap obtained from the optical data was the same as in sample A for $T \ll T_c$. This suggests that no conclusive temperature dependence of 2Δ can be obtained from our study. The ratio $2\Delta/kT_c$ for samples A and B is ~ 6, which is in good agreement with $2\Delta/kT_c \sim 5.9-6.7$ from tunneling experiments[1-4] and $2\Delta/kT_c \sim 8$ from the uv-photoemission study by Imer *et al.*[24] on $Bi_2Sr_2CaCu_2O_8$ crystals. These high values of $2\Delta/kT_c$ imply that the Bi (2:2:1:2) superconductor is a strongly coupled superconductor. Schlesinger *et al.*[25] reported a value of $2\Delta/kT_c \sim 8$ from optical studies on single-crystal samples of $YBa_2Cu_3O_{7-x}$.

In Fig. 10 we show the reflectance data of sample A in the 0–5 eV range. The low-energy reflectance data were fit to a Drude model and we obtained a plasma frequency $\omega_p = 1.9$ eV which is consistent with σ_0 and τ used in the analysis of the low-temperature data. This value for ω_p is in good agreement with $\omega_p = 1.4$ eV reported by Reedyk *et al.*[15] for single-crystal Bi (2:2:1:2) and in reasonable agreement with $\omega_p = 1$ eV reported by Tagaki *et al.*[26] for single-crystal Bi (2:3:3:2). Similar values of $\omega_p = 1.3$ eV were reported by Hughes *et al.*[8] for Bi (2:2:1:2) thin films on MgO substrates. The poor agreement between the data and the Drude model fit around 1 eV is due to the fact that no oscillators were added to fit the mid-ir electronic or interband absorption. Recently, Mattheiss *et al.*[27] calculated an electronic band structure for Bi (2:2:1:2) using the linear augmented plane-wave method. They report a relatively low total carrier density of $\sim 8.8 \times 10^{21}$ cm^{-3}. By comparing this carrier density with ω_p, we obtain an estimate of the free carrier effective mass of $\sim 3m_e$ for the in-plane carriers, where m_e is the electron mass. Consistent with the band structure of Mattheiss *et al.*,[27] we attribute the broad peak centered at 1.75 eV with the interband transitions from the nearly full O($2p$) bands to the nearly empty Cu($3d$) bands around the D point. Brorson *et al.*[28] performed femtosecond thermomodulation measurements on high-T_c superconductors using a 1.98 eV colliding pulse mode locked dye laser in a pump-probe configuration. From their study of the dynamics of the O($2p$) to Cu($3d$) band charge-transfer excitations occurring in the CuO_2 planes, we infer that the 1.75 eV peak in our reflectance spectrum corresponds to an electronic excitation of an electron from the O($2p$) to the Cu($3d^9/3d^{10}$) band. The peak centered at 3.6 eV is attributed to the transitions from the O($2p$) to the Cu($3d$) bands around the D and X points.

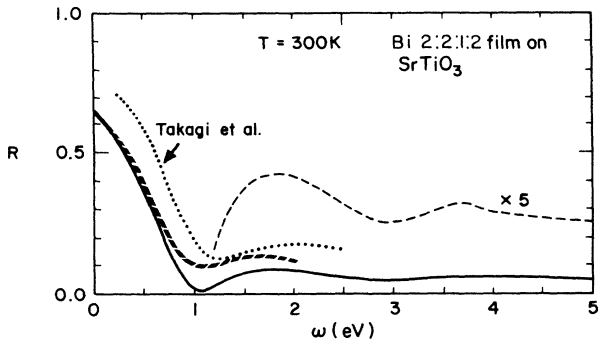

FIG. 10. Measured reflectance of sample A from 18 meV to 5 eV. The curve represented by dots is the reflectance spectrum of a Bi (2:3:3:2) single crystal obtained by Tagaki *et al.* (Ref. 26). The dashed line represents our data when magnified five times. The hatched line is a Drude fit to the reflectance data with $\omega_p = 1.9$ eV and no oscillators were used to fit the mid-ir electronic or interband absorption.

IV. CONCLUSIONS

The far-infrared reflectance of Bi (2:2:1:2) thin films on $SrTiO_3$ substrates were measured in the temperature range $5 < T < 300$ K. The results were analyzed, including the effect of the reflectance from the film-substrate interface for the optically thin Bi (2:2:1:2) films. The 5 K reflectance data were fit by using Leplae's model for the superconducting Bi (2:2:1:2) film and yield $2\Delta \sim 6k_B T_c$, which is in good agreement with 2Δ obtained from the tunneling experiments on Bi (2:2:1:2) single crystals. Normal-state reflectance data could be fit with a frequency-independent τ and similar fits to the superconducting-state reflectance indicate that the Bi (2:2:1:2) films are well characterized in the dirty limit, rather than in the clean-limit approximation. To fit the far-infrared reflectance for both the normal state and the superconducing state, two independent oscillators ($q = 0$ phonons) were required, having frequencies lower than the phonon frequencies obtained from the Bi (2:2:1:2) single crystals. The screened plasma frequency was found to be ~ 1.9 eV and yields an effective in-plane carrier mass of $3m_e$, where m_e is the free electron mass.

ACKNOWLEDGMENTS

The research at Massachusetts Institute of Technology (MIT) was supported in part by U.S. Air Force Office of Scientific Research (AFOSR) agreement BX2961 (administered through MIT Lincoln Laboratory). The research at the University of Kentucky was funded, in part, by the University of Kentucky Research Foundation, U.S. Department of Energy (USDOE) Grant No. DE-FG05-84ER45151.

APPENDIX A: LEPLAE'S EQUATIONS

In this appendix, Leplae's[9] conductivity expression in the superconducting state $\sigma_1^S(\omega) + i\sigma_2^S(\omega)$ is transformed

into expressions suitable for numerical work. The algebra is rather extensive and so we present only the results. The normal conductivity is given by the Drude expression

$$\sigma^N(\omega)=\frac{\sigma_0}{1-i\omega\tau}\ , \tag{A1}$$

so the real part $\sigma_1^N(\omega)$ is given by

$$\sigma_1^N(\omega)=\frac{\sigma_0}{1+(\omega\tau)^2}\ , \tag{A2}$$

which is an even function of ω. When $\tau=0$, our results are easily recognized to be those first derived by Mattis and Bardeen.[10]

1. Real part of $\sigma^S(\omega)$

Equation (20) of Leplae[9] should read

$$\sigma_1^S(\omega)=\frac{1}{2\hbar\omega}\int_{\Delta}^{\hbar\omega-\Delta}dE\{[g(E)+1]\sigma_1^N(|\epsilon|+|\epsilon'|)+[g(E)-1]\sigma_1^N(|\epsilon'|-|\epsilon|)\}\times\Theta(\hbar\omega-2\Delta)\ , \tag{A3}$$

where

$$g(E)=(EE'-\Delta^2)/(|\epsilon||\epsilon'|)\ ,\quad |\epsilon|=(E^2-\Delta^2)^{1/2}\ ,\quad |\epsilon'|=(E'^2-\Delta^2)^{1/2}\ , \tag{A4}$$

Θ is a unit step function, and

$$E'=\hbar\omega-E\ . \tag{A5}$$

The Mattis-Bardeen result is most easily obtained by introducing a new variable of integration u into Eq. (A3), where $-1\le u\le 1$. Let

$$\bar{\omega}=\hbar\omega/(2\Delta) \tag{A6}$$

denote a dimensionless frequency and set

$$E=\Delta[\bar{\omega}-(\bar{\omega}-1)u]\ , \tag{A7}$$

so that $E=\Delta$ and $\hbar\omega-\Delta$ when $u=1$ and -1, respectively. Then one finds that

$$\sigma_1^S(\omega)=\sigma_0[(\bar{\omega}-1)/\bar{\omega}]\int_0^1 du\frac{G(u)}{[(1-u^2)(1-k^2u^2)]^{1/2}}\ , \tag{A8}$$

where

$$G(u)=\frac{1+[(1+k^2-2k^2u^2)c-k]u^2}{C+Bu^2}\Theta(\bar{\omega}-1)\ ,\quad c=2(\Delta\tau)^2(\bar{\omega}^2-1)\ ,\quad C=1+2c\ ,\quad B=c[2k+(1+k)^2c]\ , \tag{A9}$$

where

$$k=(\bar{\omega}-1)/(\bar{\omega}+1),\quad 0\le k\le 1 \tag{A10}$$

is the usual symbol for the modulus of the complete elliptical integrals, $\mathcal{E}(k)$ and $\mathcal{K}(k)$.

To get the Mattis-Bardeen[10] result ($\Delta\tau=0$), one writes

$$1-ku^2=[(k-1)/k]+[(1-k^2u^2)/k]$$

and obtains

$$\sigma_1^S(\omega)=\sigma_0\Theta(\bar{\omega}-1)[(\bar{\omega}+1)\mathcal{E}(k)-2\mathcal{K}(k)]/\bar{\omega}\ , \tag{A11}$$

where

$$\mathcal{E}(m=k^2)=\int_0^1 du[(1-mu^2)/(1-u^2)]^{1/2} \tag{A12}$$

and

$$\mathcal{K}(m=k^2)=\int_0^1 du[(1-mu^2)(1-u^2)]^{-1/2}\ . \tag{A13}$$

In Eq. (A12), $\mathcal{E}(k^2)$ denotes the well-known complete elliptical integrals of the first kind while $\mathcal{K}(k^2)$ in Eq. (A13) relates to the second kind of elliptic integrals. In a recent paper by Thomas *et al.*[29] it appears that they used $m=k$ instead of $m=k^2$ in Hasting's approximation for $\mathcal{E}$ and $\mathcal{K}$, presumably leading to errors in their calculations.

One might also note that $\sigma_2^S(\omega)$ for $\Delta\tau>0$ can be written in terms of $\mathcal{E}(k^2)$ and $\mathcal{K}(k^2)$, and a complete elliptical integral of the third kind. But this integral is not easily evaluated. Hence, we evaluate Eq. (A8) by using a Gaussian quadrature, after removing the ill-behaved factor $[(1-u)(1-ku)]^{1/2}$ in the denominator of Eq. (A8).

2. Imaginary part of $\sigma^S(\omega)$

When $\Delta\tau=0$, we know that $\sigma_2^S(\omega)$ must reduce to the Mattis-Bardeen (MB) result

$$\sigma_{2,\mathrm{MB}}^S(\omega)=\tfrac{1}{2}[(1+x)\mathcal{E}(k')+(x+1)\mathcal{K}(k')]\sigma_0\ , \tag{A14}$$

where

$$x=1/\bar{\omega}\ \text{and}\ k'=(1-k^2)^{1/2}\ . \tag{A15}$$

Equation (A14) was used to check our numerical results when $\Delta\tau=0$.

From Leplae, one finds that

$$\sigma_2^S(\omega)=\frac{2A}{\pi\bar{\omega}}-\frac{2\bar{\omega}}{\pi}P\int_1^{\infty}d\bar{\omega}'\sigma_1^S(\bar{\omega}')/(\bar{\omega}'^2-\bar{\omega}^2)\ , \tag{A16}$$

where

$$A=\int_{0+}^{\infty}d\bar{\omega}[\sigma_1^N(\bar{\omega})-\sigma_1^S(\bar{\omega})]\ , \tag{A17}$$

P is the principal value and $\bar{\omega}$ is defined in Eq. (A6).

The A integral is split into two parts and $\bar{\omega}=1/x$ is used for the $1\le\bar{\omega}\le\infty$ part. Hence,

$$A=\frac{\arctan(2\Delta\tau)}{2\Delta\tau}+\int_0^1\frac{dx}{x^2}[\sigma_1^N(1/x)-\sigma_1^S(1/x)] \tag{A18}$$

and a 32nd-order Gaussian quadrature was used to evaluate this integral numerically.

The final result can be written as

$$\sigma_2^S(\bar{\omega})=\frac{2A}{\pi\bar{\omega}}-\frac{\sigma_1^S(\bar{\omega})}{\pi}\ln[(\bar{\omega}+1)/(\bar{\omega}-1)] - \frac{2\bar{\omega}}{\pi}\int_0^1 dx[\sigma_1^S(1/x)-\sigma_1^S(\bar{\omega})]/[1-x^2\bar{\omega}^2] . \quad \text{(A19)}$$

In the limit $\Delta\tau\rightarrow 0$, our results agree with those of Mattis-Bardeen,[10] Eq. (A14).

Another good check is provided by the requirement that

$$\sigma_2^S(\bar{\omega})\rightarrow 1/(\omega\tau) , \quad \text{(A20)}$$

the usual result when $(\omega\tau)\gg 1$.

---

*Present address: Physics Department, Massachusetts Institute of Technology, Cambridge, MA 02139.

†Present address: E. I. duPont Corporate Research Center, Wilmington, DE 19880.

‡Present address: Physics Department, General Motors, Warren, MI 48090.

[1]N. Miyakawa, D. Shimada, T. Kido, and N. Tsuda, J. Phys. Soc. Jpn. **58**, 383 (1989).

[2]N. Miyakawa, D. Shimada, T. Kido, and N. Tsuda, J. Phys. Soc. Jpn. **58**, 1141 (1989).

[3]D. Shimada, N. Miyakawa, T. Kido, and N. Tsuda, J. Phys. Soc. Jpn. **58**, 387 (1989).

[4]M. Lee, D. B. Mitzi, A. Kapitulnik, and M. R. Beasley, Phys. Rev. B **39**, 801 (1989).

[5]U. Walter, M. S. Sherwin, A. Stacey, P. L. Richards, and A. Zettl, Phys. Rev. B **35**, 5327 (1987).

[6]Z. Schlesinger, R. L. Greene, J. G. Bednorz, and K. A. Muller, Phys. Rev. B **35**, 5334 (1987).

[7]T. Timusk and D. B. Tanner, *Physical Properties of High Temperature Superconductors I,* edited by D. M. Ginsberg (World Scientific, Singapore, 1989), Chap. 7, p. 341.

[8]R. A. Hughes, T. Timusk, S. L. Cooper, G. A. Thomas, J. J. Yeh, and M. Hong, Phys. Rev. B **40**, 5162 (1989).

[9]L. Leplae, Phys. Rev. B **27**, 1911 (1983).

[10]D. C. Mattis and J. Bardeen, Phys. Rev. **11**, 412 (1958).

[11]F. Wooten, *Optical Properties of Solids* (Academic, New York, 1972).

[12]A. S. Barker, Jr., and J. J. Hopfield, Phys. Rev. **135**, A1732 (1964).

[13]A. S. Barker, Jr., Phys. Rev. **145**, 391 (1966).

[14]A. S. Barker, Jr., and M. Tinkham, Phys. Rev. **125**, 1527 (1962).

[15]M. Reedyk, D. A. Bonn, J. D. Garret, J. E. Greedan, C. V. Stager, T. Timusk, K. Kamaras, and D. B. Tanner, Phys. Rev. B **38**, 11 981 (1988).

[16]O. E. Piro, J. A. Guida, N. E. Massa, P. J. Aymonino, E. E. Castellano, H. C. Basso, J. N. H. Gallo, and A. A. Martin, Phys. Rev. B **39**, 7255 (1989).

[17]R. T. Collins, Z. Schlesinger, F. Holtzberg, P. Chaudhari, and C. Feild, Phys. Rev. B **39**, 6571 (1989).

[18]G. L. Carr, S. Perkowitz, and D. B. Tanner, in *Infrared and Millimeter Waves,* edited by K. J. Button (Academic, New York, 1985), Vol. 13, p. 171.

[19]D. Karecki, R. E. Pena, and S. Perkowitz, Phys. Rev. B **25**, 1565 (1982).

[20]D. R. Karecki, G. L. Carr, S. Perkowitz, D. U. Gubser, and S. A. Wolf, Phys. Rev. B **27**, 5460 (1983).

[21]D. A. Bonn, C. V. Stager, J. E. Greedan, T. Timusk, M. G. Doss, S. L. Herr, K. Kamaras, C. D. Porter, D. B. Tanner, J. M. Tarascon, W. R. McKinnon, and L. H. Green, Phys. Rev. B **35**, 8843 (1987).

[22]M. S. Sherwin, P. L. Richards, and A. Zettl, Phys. Rev. B **37**, 1587 (1988).

[23]A. Wittlin, A. Genzel, M. Cardona, M. Bauer, W. Konig, E. Garcia, M. Barahona, and M. V. Cabanas, Phys. Rev. B **37**, 652 (1988).

[24]J. M. Imer, F. Patthey, B. Dardel, W. D. Schneider, Y. Baer, Y. Petroff, and A. Zettl, Phys. Rev. Lett. **62**, 336 (1989).

[25]Z. Schlesinger, R. T. Collins, D. L. Kaiser, and F. Holtzberg, Phys. Rev. Lett. **59**, 1958 (1987).

[26]H. Tagaki, H. Eisaki, S. Uchida, A. Maeda, S. Tajima, K. Uchinokura, and S. Tanaka, Nature **332**, 236 (1988).

[27]L. F. Mattheiss and D. R. Hamann, Phys. Rev. B **38**, 5012 (1988).

[28]S. Brorson, A. Kazeroonian, D. W. Face, T. K. Cheng, G. L. Doll, M. S. Dresselhaus, G. Dresselhaus, E. P. Ippen, T. Venkatesan, X. D. Wu, and A. Inam, Solid State Commun. (to be published).

[29]G. A. Thomas, H. K. Ng, A. J. Millis, R. N. Bhatt, R. J. Cava, E. A. Rietman, D. W. Johnson, Jr., G. P. Espinosa, and J. M. Vandenberg, Phys. Rev. B **36**, 846 (1987).